NASA/CR—1999-208873

Low–Energy Sputtering Studies of Boron Nitride with Xenon Ions

P.K. Ray and V. Shutthanandan
Tuskegee University, Tuskegee, Alabama

National Aeronautics and
Space Administration

Lewis Research Center

January 1999

Available from

TABLE OF CONTENTS

LIST OF FIGURES

LIST OF TABLES

1. INTRODUCTION

The stationary plasma thrusters (SPT) using xenon have been successfully developed in the former Soviet Union into a very efficient space propulsion device [1,2]. The SPTs offer thrust levels that are superior to other electric thrusters in the specific impulse range of 1000 to 2000 s at low power levels at a high efficiency. This range of specific impulse is of interest to many missions in the near-Earth-space. Performance measurements of these thrusters have been made at NASA's Lewis Research Center and the Jet Propulsion Laboratory to evaluate the engineering issues [3-5]. The SPT plume characteristics have also been investigated. The electron number density and temperature throughout the thruster plume have been measured [6] and optical diagnostics have been used to identify the plume signature [7].

The walls of SPT discharge chambers are typically made of ceramic insulating materials. Borosil, a mixture of boron nitride, silicon dioxide, and several other dielectric, is a typical SPT insulator material as it provides high melting point, good mechanical properties, high resistivity and high thermal conductivity. However, long-duration tests have indicated significant sputtering erosion of the discharge chamber walls [2-5,8]. The sputtered material has been observed in the SPT plume. This results in the contamination of spacecraft surfaces and solar panels. Hence, the sputtering of discharge chamber walls influences the optimization of the thruster-spacecraft integration design. Samples have been placed in the plume to measure erosion as well as depositions on them [9-11].

In an SPT, inert gas is injected into both the hollow cathode and the main discharge chamber. A discharge voltage of about 300 V is applied between the anode and the cathode. Ions are created in the discharge chamber by electron bombardment of the propellant atom. A radial magnetic field is established across the annular channel of the main discharge region. The radial

magnetic field forces the electrons emitted from the cathode to spiral around the magnetic field lines. This impedance to the flow of electrons serves to establish most of the applied potential difference between the anode and the cathode across the magnetic field. The result is an electric field which is largely axial and which serves to accelerate the ions. Additional electrons are drawn from the cathode by the resulting ion beam and provide current neutralization [2].

The SPT walls are subjected to bombardment by ions contained in a plasma potential of approximately 300 V. A small fraction of these ions could be in the doubly-charged state. Thus, the walls of the discharge chamber are bombarded by ions having energies up to 600 eV. However, to the best of our knowledge, no sputtering related information is available for borosil and very little, for its major component, boron nitride [12].

We have performed a systematic investigation of sputtering of boron nitride by xenon ions at energies below 3 keV. The objective of this research was to set up an experimental assembly to bombard boron nitride with low-energy xenon ions and study the characteristics of the material sputtered form it as a function of the primary ion energy under well-defined experimental conditions. When a solid surface is bombarded by energetic particles, emission of atoms, molecules, electrons, and photons from the target surface is observed. The sputtered atoms and molecules are ejected as neutrals and ions (both positive and negative) and also, in excited states. For this study, an instrument, which can be operated in both secondary ion (SIMS) and secondary neutral (SNMS) mass spectrometry modes, was utilized. This allowed us to study the emission of sputtered neutrals as well as positive and negative secondary, molecular and cluster ions in one experiment by changing electrode potentials on the spectrometer.

This report is divided into four parts. The first part represents a summary of the literature search on the techniques involved in the sputtering of insulators in general. The next chapter

briefly describes the experimental set-up. The measurement of sputtered neutrals as well as positive and negative secondary, molecular and cluster ions are described next.

While performing these experiments, we observed that heavy isotopes are sputtered preferentially over light isotopes at low energies when xenon was used as the primary ion. This is contrary to the usual observation of preferential emission of light isotopes in the sputtering process. We have investigated this aspect of preferential sputtering by bombarding boron nitride with xenon ions with energies ranging from 100 eV to 1.5 keV. The results are also presented in this report.

2. SPUTTERING OF INSULATORS - LITERATURE REVIEW

Literature searches have been carried out to determine the state-of-the-art work in the area of sputtering of insulators. Despite the existence of a large body of data obtained from a variety of experiments, the sputtering of multicomponent targets by ion bombardment is not fully understood because it is often associated with surface composition changes due to preferential sputtering of one component over the others [13]. The short review presented below indicates the current status of experimental work on the sputtering of insulators which is relevant to the present work.

Positive ion bombardment of an insulating target produces charged layers on the target surface. As surface charges build up, it affects the impact parameters of the primary beam as well as the energy distribution of the ejected species. Simple remedies like a very low primary ion current or sample heating to improve its conductivity are unattractive for reasons of loss of sensitivity and diffusion-induced profile alteration [14]. One way this problem can be avoided is to coat the surface of the target with a thin metallic layer. The other is to expose the target continuously to a beam of energetic (~ 0.1 to 1 keV) electrons from an electron gun. This method works reasonably well. However, the electron beam current must be tuned to each new target material, a problem in insulating multilayer samples. Finally, defocusing or rastering over an area in excess of ion irradiated area is usually necessary.

In early studies of sputtering of insulators, sputtering of Ta_2O_5 of about 3500 A thickness has been studied by Oechsner et al [15]. In this work a secondary neutral mass spectrometer (SNMS) was use to study the ion induced neutral particle emission from anodically formed Ta_2O_5 layers. A low pressure, high frequency plasma was used for ion bombardment of a negatively biased target inside the discharge as well as for postionization of the sputtered neutral particles. The current density of the normally incident bombarding Ar^+ ions at the target was in the range of 2-3 mA/cm^2. The ion energy was varied between 50 and 900 eV. By using the depth

4

measurements (i.e., the total ion dose necessary to remove the entire thickness of the oxide layers), the total and partial sputtering yields were determined.

From these measurements it was concluded that the dominating peaks in the mass spectra of postionized neutral particles sputtered from Ta_2O_5 by low energy Ar^+ ions belong to Ta and TaO. Hence, Ta_2O_5 can be considered to be sputtered mainly as neutral TaO and Ta and from stoichiometric arguments as charged or neutral atomic or molecular oxygen. The partial sputtering yield of Ta, TaO, and O sputtered from Ta_2O_5 was derived from these measurements. For normal bombardment with Ar ions of 100 to 600 eV, the partial sputtering yield of TaO and the partial oxygen yields were about 4 and 7 times higher than the partial sputtering yield of Ta. Similar behavior is also observed for other metal oxides like Nb and W. In a different approach, Mamoru et al showed that the sputtering rate of the Ta_2O_5 is 2-5 times higher than that of Al_2O_3 and SiO_2 [16]. In their work, they studied the dielectric properties (breakdown voltage) of these insulators as a function of the film thickness at different sputtering conditions.

The total sputtering yield (in atoms/ion) of Ta_2O_5 measured by Oechsner et al was found to be more than that of the sputtering yield of the clean metal. For Ar^+ ions of 500 eV, a sputtering yield ratio (S_{total}/S_{metal} - Ta) of 2.2, was obtained.

The use of low-pressure rf plasma sputtering on non conductive powders was studied by Dang et al [17]. Powders of various shapes and sizes including latex spheres, Y_2O_3, Zn_2SiO_4, $BaSi_2O_5$ and ZrO_2 have been used in this study. The potential build up during sputtering of non conductive materials can cause dielectric breakdown and non uniform sputtering. To prevent this, the powders were dispersed in a silver paint which is a conductive medium.

The experimental system consisted of an inductively rf-excited argon plasma. A negative bias of 500 V applied to the target resulted in the extraction of Ar^+ ions from the plasma to the sample's surface. The sputtered neutrals diffused into the plasma where it was postionized by electrons generated in the plasma and subsequently analyzed by a quadrupole mass analyzer. A uniform erosion rate was observed in the sample after the sputtering was completed.

Plasma-based secondary neutral mass spectrometry was found to be appropriate to measure the elemental composition of particulate material containing oxides, salts or organic compounds [18]. In a recent experiment, a metal foil supporting impressed powder grains was mounted behind an orifice in the wall of a chamber containing a rf-excited argon plasma [19]. A negative voltage applied to the metal carrier accelerated argon ions out of the plasma towards the sample. The argon pressure of the plasma was set to 2×10^{-3} mbar. The primary ion current density incident to the samples was determined to be 0.6 - 1.0 mA/cm^2.

Several salts and some oxides were chosen to be investigated. Regular grade powders (particle size < 100 µm) were pressed into indium foil covering less than half of the plasma exposed area (7 mm in diameter). Keeping the coverage lower than this limit turned out to be sufficient to avoid interference of the measurements by charging. However, with the same salts in compact form, such as pressed tablets, nearly no sputtering was possible due to severe charging of the electrically insulating material under ion bombardment.

Formation of F$^+$ in sputtering of LiF has been studied using He$^+$, Ar$^+$ and Xe$^+$ ions and their neutral atoms with kinetic energies ranging between 250 eV and 1 keV [20]. The sample was held at a temperature of 400^{0}C to prevent charging and to keep the surface stoichiometric [21]. The experiments show that F$^+$ is formed not only by Auger neutralization of the primary particle but also very efficiently by kinetic processes during the primary particle-fluorine collision.

Sputtering and crater formation in garnets were studied by Priggemeyer et al [22,23]. Garnets are oxidic materials and have potential in magneto-optical applications including optical waveguides. An Ar$^+$ ion beam of diameter 0.2 mm was used with an energy of 4.5 up to 15 keV. To compensate the charging of the surfaces an electron gun with a primary energy between 3 and 4.5 keV was used. The diameter of the electron beam was about 15 mm. Insufficient charge compensation was found to cause irregular craters.

One interesting question in the sputtering of insulators is the influence of the potential energy of the projectile on the ejection of larger atoms. This should be noticeable at very low

impact energy, where all processes induced by ballistic sputtering are drastically reduced. To study this effect, total sputter yields of LiF induced by singly charged rare gas ions He$^+$, Ne$^+$ and Ar$^+$ with a kinetic energy of 5-500 eV were measured [24]. The target was evaporated on the quartz crystal of a micro balance. The rate of material removal was determined from the frequency change of the crystal. The results show a large and slowly decreasing total sputtering yield at low energies. This fact was interpreted as evidence for electronic processes in the sputtering of LiF.

One of the problems associated with depositing and subsequently sputtering material from quartz crystals is the energy deposited by primary particles onto the sputtered surface, causing problems of thermal drift. Energy, ranging from few eV to several hundred eV per sputtered atom, can be deposited on the sputtered surface. The problem of energy deposition by the ion beam can be avoided by using the quartz crystal as a collector for sputtered material. In this mode of operation, the energy deposition per incident atom is only a few eV from the sublimation energy. This technique was used in the sputtering of oxides and alkali halides by Betz and Husinsky [25].

The spatial distribution of material removal by directed-ion-beam sputtering was investigated by Weeiser [26]. In this study, ions of neon, argon and krypton were used to sputter glass. A 3 cm gridded, broad beam ion source of the Kaufman-type was used in this study. The energy of the ions ranged from 300 to 1000 V.

The material removal rate was monitored by direct measuring interferometry and a high-resolution laser interferometer. The charge build-up on the sample was avoided by resonant charge exchange whereby the energetic ions were scattered by the residual gas molecules and atoms while losing their positive charge. As a result only neutral energetic atoms impinged on to the substrate. However, to achieve this condition, relatively high pressures (10^{-4} -10^{-3} Pa) must be employed.

Sputtering of solid nitrogen with low energy (4 -10 keV) helium ions (3He+ and 4He+) was investigated by Ellegaard et al [27]. Films of 3-5 x 10^{17} molecules/cm^2 of solidified nitrogen

were produced by letting a jet of cooled gas impinge on an oscillating quartz crystal. The absolute sputtering yields were evaluated from the frequency shift of the microbalance. The yields were found to depend weakly on the primary energy and the isotopic mass.

Desorption of positive and negative ions for electron and ion bombarded NaCl crystals was investigated by Postawa et al [28]. The sample was bombarded with a 0.6 - 5 keV electron beam and a 0.6 - 5 keV argon ion beam. To avoid charging, the target surface was covered by a fine molybdenum mesh and measurements were made at elevated temperature (430 K). This temperature was high enough for the surface to remain stoichiometric during irradiation [29]. Sputtered positive and negative ions were found to be created by direct ejection of lattice ions from the collision cascade.

An electron beam excited plasma was utilized for sputtering studies with an SNMS in a system called SNART (Sputtered Neutral Analysis-Riken Type) [30]. It was observed that the potential difference between the floating potential and the space potential was sufficiently large for sputtering. Depth profiles of ZnS film were obtained with 110-eV Ar^+ bombardment at a high sputter rate of 12.5 nms^{-1}. Relative sensitivity factors in insulator analysis were established and found to deviate in a small range in contrast to SIMS.

Sputter deposited thin film of $Pb(Mg_xNb_{1-x})O_y$ has been studied by Pignolet et al [31]. Different deposition conditions were varied and their effects on the film composition and compositional uniformity were investigated by Rutherford backscattering spectroscopy (RBS). Sputtering yields for Pb (2.3), Nb (0.6), Nb_2O_5 (0.22), Mg (0.29), MgO (0.33), for 500 eV Ar ions at normal incidence were obtained from this experiment. The sputter yields are expressed in terms of ratio of species removed per incident ion. MgO films deposited using off-axis magnetron sputtering revealed a sputtering (deposition) rate of 0.4 nm/min [32]. A high pressure (10 - 20 Pa) of pure Ar were used during this sputtering process.

The approach taken by Jongmin et al to characterize oxide layers in Al thin film devices was to use X-ray photoelectron spectroscopy (XPS) with sputter depth profiling [33]. This method provides a direct measure of the atomic concentration of oxide at any given depth in a

film. From this method sputter rate of 1.4 nm/min was observed for oxidized aluminum (Al_2O_3). They further concluded that the sputter yield of oxidized aluminum is 6-8 times lower than that of pure aluminum metal. Usually the sputtering yield, Y (atoms/ion) is proportional to the sputtering rate S (A/min) and the density d(g/cm^3) and inversely proportional to the ion beam current density J (~μA/cm^2) and atomic or molecular weight A(g) and it is given by the following equation Y= Sd/(0.06JA) [34]. Hence using this equation the sputter rates can be converted to sputtering yields.

The use of thin films of boron nitride (BN) in the electronics industry has been the subject of considerable research [35]. BN is used as a high temperature thermal and electrical insulator because of its high melting point, good mechanical properties, high resistivity and high thermal conductivity. Its crystalline phases are analogous to the carbon phases. The hexagonal BN (h-BN) has a layered structure like graphite, in which boron and nitrogen atoms are at the vertices of hexagonal which are fused together forming planar sheets. The B-N bonds have covalent sp^2 hybridization with π electrons above and below the planes. On the other hand, cubic BN (c-BN) is the analog of cubic diamond and is the second hardest material following diamond. It has the zinc blende lattice structure and its B-N bonds, like diamond, have strong sp^3 hybridization.

The study of the effect of subjecting c-BN and h-BN to bombardment by N_2^+ and Ar^+ ions was conducted by Trehan et al [12]. This study was interesting in view of the fact that Ar^+ ion bombardment of a diamond surface can cause amorphization or graphitization [36]. Auger electron spectroscopy and X-ray electron spectroscopy were used to probe the local bonding state (sp^2 or sp^3) of BN formed by the irradiation of 1 and 4 keV N_2^+ ions on a clean boron as well as the behavior of these two forms of BN under Ar^+ ion bombardment. There were significant differences in the Auger line shapes and core-level XPS loss features between h-BN and c-BN for both N and B spectra. These features are sufficiently different for the AES and XPS spectra to be used as "finger prints" of the h-BN (sp^2) and c-BN (sp^3) structures.

The changes observed in the XPS and the Auger spectra upon 1 to 4 keV ion bombardment of c-BN reveals that N_2^+ bombardment of c-BN changes the local bonding environment of B and N from sp^3 type to sp^2 type characteristic of the hexagonal phase without changing the stoichiometry. Bombardment of h-BN with 1 or 4 keV Ar^+ or N_2^+ ions does not produce any significant changes in the Auger or XPS line shapes. It was observed that the broadening and smearing of peaks in the Auger spectrum and plasmon loss peaks in the XPS spectrum become weaker. These changes may be attributed to amorphization of the h-BN sample. N_2^+ ion bombardment of B at 1 and 4 keV energies leads to BN which has hexagonal like bonding characteristics.

3.   EXPERIMENTAL SET-UP

The experimental setup is shown schematically in Fig.1. The major components of the experimental system and some operating parameters are described below.

3.1   Vacuum system

The experiments were performed inside a spherical vacuum chamber. The diameter of the chamber was 22.5 cm. A 170 liter/sec, 2-stage turbomolecular pumping system was used to provide the required vacuum conditions. The pump can attain a base pressure in the region of 1×10^{-9} Torr inside the chamber. The pressure inside the chamber was monitored by a hot cathode ionization gage. A gate valve was incorporated between the vacuum chamber and the turbomolecular pump to isolate the pump from the vacuum chamber as needed.

3.2   Ion gun assembly

An ion gun (model ILG-2), built by Kimball Physics Inc., was used in the present investigation. The ion gun has the capability of generating noble gas ions such as xenon and argon in the energy range 10 eV to 3 keV. The gas enters the ion gun through a port multiplexer. Xenon gas of 99.999% purity was used in our experiments. A uniform ion beam current was maintained by a stabilized gas flow system. When xenon was introduced into the vacuum chamber, the pressure increased to 1×10^{-6} Torr.

The ion gun can deliver a beam current of 0.005 μA at 10 eV and 0.35μA at 500 eV. The ion beam can be focused on a target at a distance of 20 mm from the exit plane. The size of the focused beam is approximately 1 mm in diameter. A Raster Generator Deflection Unit was used to move the beam on the target surface. This unit is capable of rastering the beam both along the x- and the y- axes in a 4 mm x 4 mm area.

Electron Gun

Ion Gun

SNMS/SIMS

Sample

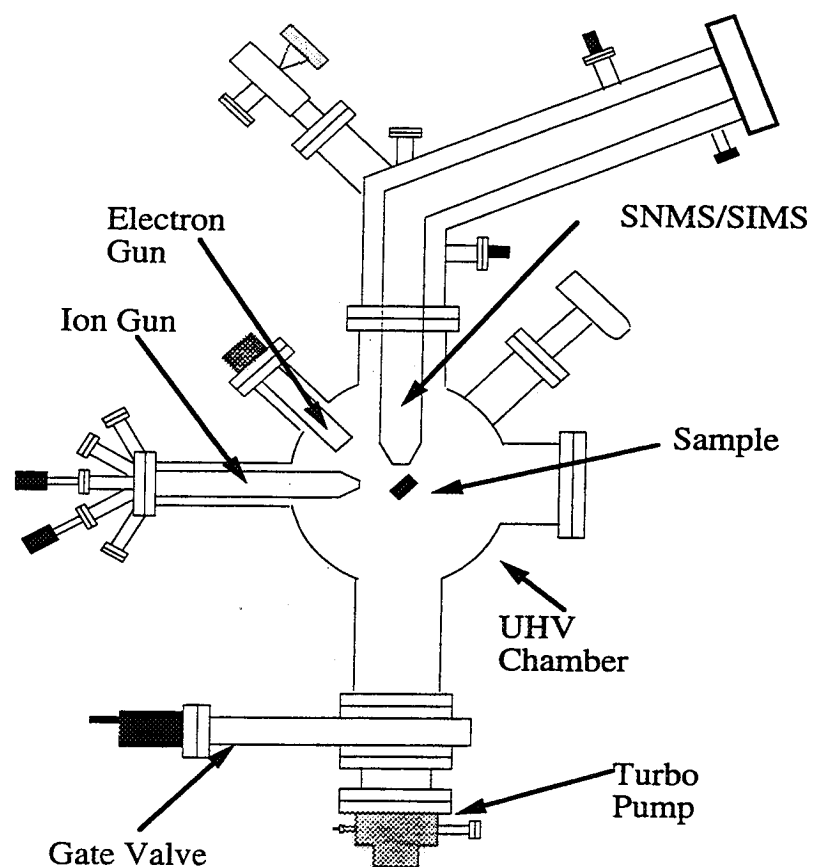UHV Chamber

Turbo Pump

Gate Valve

Fig. 1.   Schematic diagram of the experimental arrangement

The ion current was measured by a Faraday cup which was mounted on the ion gun. It could be actuated pneumatically to intercept the ion beam at a distance of 6 mm from the exit plane of the ion gun. The Faraday cup was interfaced with an electrometer to provide the ion current reading.

3.3   Mass spectrometer

A mass spectrometer (model SSM 200), built by SPECS Inc., was used to measure sputtering yields of molybdenum at low ion energies. The spectrometer has the capability of operating in the following modes: (i) secondary neutral mass spectrometry (SNMS), (ii) secondary ion mass spectrometry (SIMS), (iii) residual gas analysis (RGA), and (iv) thermal desorption mass spectrometry. The major components of the spectrometer is depicted schematically in Fig. 2.

In the SNMS mode of operation, the sputtered neutrals are ionized by electron impact in a region defined by the ionizer inside the spectrometer. The ionization of the sputtered neutrals was performed by a 5 mA electron beam at 50 eV. The residual gas particles which are also ionized possess kinetic energies in the 0.001 to 0.1 eV range and are prevented from entering the mass filter by applying an appropriate retarding electric field. The postionized neutrals, which have energy in the 1 to 10 eV range, are subsequently mass analyzed by a quadrupole system and detected by a single channel electron multiplier. During the operation of the spectrometer in the SNMS mode, positive secondary ions are electrostatically deflected before they can reach the ionizer volume and negative secondary ions are removed by the optical system since all functional elements are set to transport positive ions only. The spectrometer can effectively collect and separate secondary ions, postionized neutrals and residual gas signals from each other at a very high dynamic ratio.
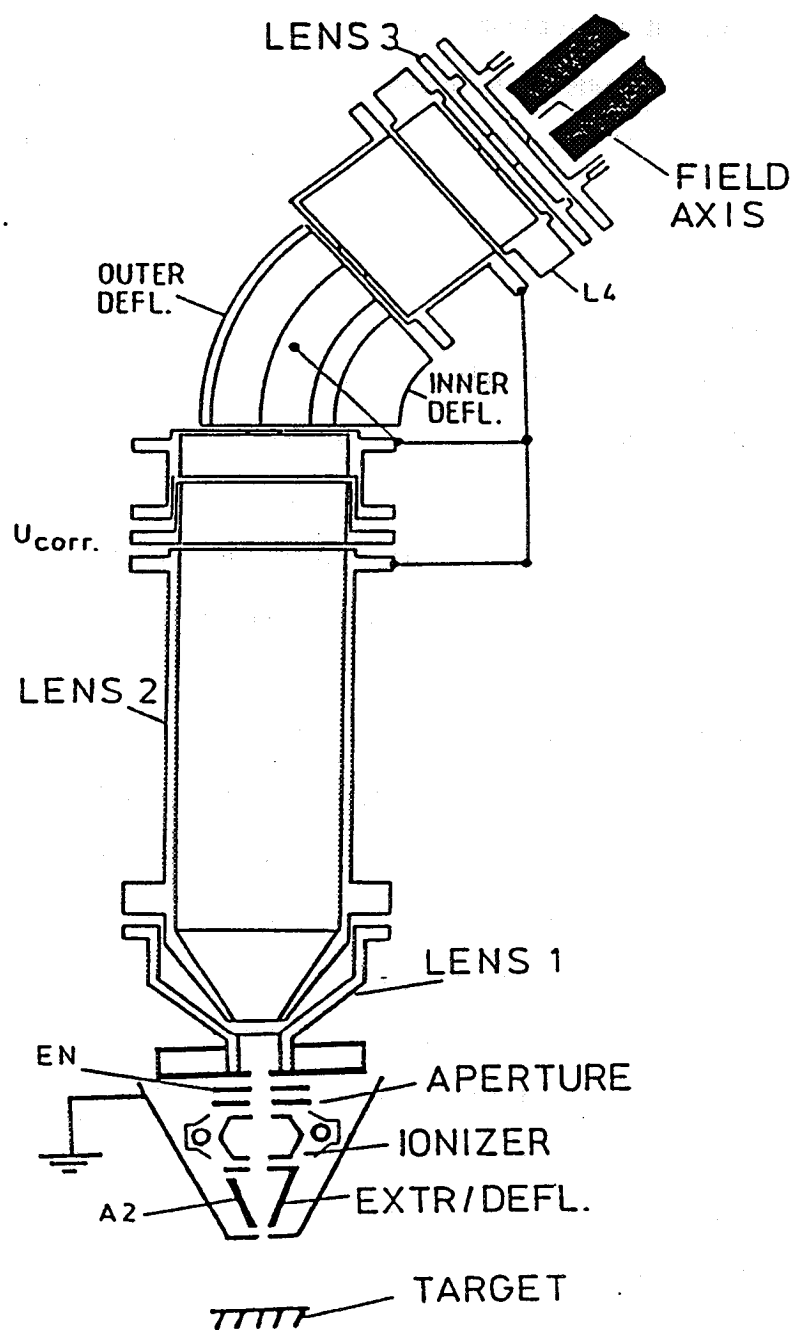
13

Fig. 2. Schematic diagram of the mass spectrometer

Two lenses (LENS 1 and LENS 2) are used to focus the ionized particles from the ionizer volume to the front of the energy analyzer. An electrostatic energy filter serves to transport ionized neutrals to a third lens (LENS 3) and filter out all uncharged particles coming from the ionizer region. The energy analyzer also suppresses a majority of ionized residual gas molecules that are not blocked by the retarding field. The focusing of charged particles leaving the energy filter into the quadrupole mass filter is controlled by LENS 3. The transfer lens (L4) operates as an accelerating immersion lens and focuses the charged particles into the quadrupole rod system.

The high transmission quadrupole system with a mass range of 0-511 amu is controlled by the data acquisition unit connected to a computer. The mass filter consists of four cylindrical rods arranged symmetrically to the z-axis. Each pair of opposite rods in connected between two pairs of rf voltage with superimposed dc voltage. The ions injected into the mass filter in the z-direction are stimulated by electric field to oscillate in x and y direction. The proper selection of voltages enables ions of a particular charge-to-mass ratio to emerge out of the system for detection by a secondary electron multiplier capable of handling count rates in excess of 5×10^6 cps. The output pulses of the electron multiplier, after further amplification and discrimination, are fed to a computer for data evaluation and storage.

3.4   Charge neutralization

Since boron nitride is an insulator, the impact of positively charged ions leads to a positive charge build-up on the target surface. This charge build-up not only changes the energy distribution of the sputtered ions, but also changes the energy of incoming ions. A flood electron gun was used in our experiments to neutralize the positive charge build-up on the target surface. It was observed that SNMS signals at different ion energies were not very sensitive to the energy and intensity of the electron beam. In contrast, both positive and negative SIMS spectra exhibited a strong dependence on electron current and a weak dependence on the electron energy.

Throughout this study, an electron energy of 300 eV was used in all modes of operations. In the SNMS mode, an electron beam current of 1mA was used to neutralize the positive charge build-up on the target surface. However, in the SIMS mode, different electron beam currents were used at different ion energies. For a particular incident ion energy, the B^+ (positive SIMS mode) and BN^- (negative SIMS mode) secondary ion signals were maximized at first by changing the electron current and spectra were acquired subsequently.

4. SPUTTERING INVESTIGATION OF BORON NITRIDE WITH SECONDARY ION AND SECONDARY NEUTRAL MASS SPECTROMETRY

The SIMS and SNMS spectra of boron nitride sputtered by xenon ions in the 100 eV to 3 keV energy range are reported in this section. In the present geometrical arrangement, no sputtering could be detected below 100 eV in the SIMS mode and 300 eV in the SNMS mode. Intensities of sputtered neutral and charged particles, including single atoms, molecules, and clusters as a function of ion energy are also presented.

4.1 Experimental procedure

At low incident ion energies, yields of secondary ions are significantly reduced. Moreover, the aperture of the mass spectrometer intercepts only a small amount of secondary ions sputtered from the sample. In our experiment, xenon ions impinged on the target surface at 50° angle to the surface normal. This arrangement was chosen because at this incident angle the sputtering yields are higher compared to normal incidence. The spectrometer entrance aperture was located perpendicular to the ion beam direction and 10 mm away from the target surface. In this geometric arrangement, the aperture of the spectrometer subtended a solid angle of 0.03 sr at the center of the target.

The boron nitride target was mounted on a XYZθ manipulator for precise positioning within the vacuum chamber. During sputtering, the target was placed at a distance of 20 mm from the exit plane of the ion gun. At this position, the ion beam could be focused to a spot approximately 1 mm in diameter. The beam current remained essentially constant from 150 eV to 3 keV at 0.22 μA and dropped to 0.19μA at 100 eV. Based on the 1 mm spot diameter, the ion current density at the target was 30 μA/cm^2.

The boron nitride target was 25 mm in diameter and 3 mm thick. It was supplied by Kurt J. Lesker Company. It consisted of 99.874% boron nitride in polycrystalline form. The impurities were Al (50 ppm), Si (500 ppm), Ca (450 ppm), Fe (50 ppm), Mg (20 ppm), Mn (6 ppm), and Ti (5 ppm).

SIMS and SNMS spectra were collected by bombarding the target with xenon ions at an angle of incidence of 50° with respect to the surface normal. The target was first sputter cleaned for 30 minutes using a 2.5 keV rastered ion beam. The rastered area is approximately 4 mm x 4 mm in size. The material removed from the target surface during this process is estimated to be 60 nm. The analysis was performed immediately following the sputter cleaning process with the ion beam focused at the center of the cleaned area. The operation of the system in all three modes were accomplished by optimizing the ion optics parameters of the spectrometer to obtain maximum signal intensities. In the SNMS mode, the sputtered neutrals were ionized in the ionizer by a 50 eV electron beam at an emission current of 5 mA.

4.2   Results and discussion

Data at each energy were collected over a period of 60 s in SIMS and 350 s in SNMS measurements. It is estimated that the maximum target thickness that was sputtered away during SIMS experiments was less than 2 nm. The corresponding values for SNMS experiments were 1 nm at 300 eV and 6 nm at 3 keV. Data at each energy were collected using a sweep rate of 1 amu/s in SIMS and 0.5 amu/s in SNMS modes. SIMS spectra at each energy were collected over a single scan. However, SNMS signals were weaker and hence, were accumulated over 25 scans. The mass ranges scanned were 0 to 60 amu in SIMS and 8 to 15 amu in SNMS measurements. No signal was observed beyond 60 amu in SIMS and 15 amu in SNMS modes of operation.

In SIMS measurements, spectra related to boron nitride were observed only in the 0-25 amu mass range. Beyond 25 amu, the signals consisted of positive ions of impurities in the target such as Al, Ca, etc. Hence, only partial SIMS spectra in the 0-25 amu mass range are presented here.

4.2.1. Positive SIMS spectra

The positive SIMS (p-SIMS) spectrum of boron nitride under xenon ion bombardment at 2 keV is shown in Fig. 3. The spectrum clearly identifies the two boron isotopes, ^{10}B and ^{11}B. Molecular ions such as $^{10}B_2^+$ and $^{11}B_2^+$, cluster ions such as $(^{11}B+^{10}B)^+$ and BN^+ are also observed, although at a much lower intensity level. The spectrum also reveals the presence of Na in the target. Although it was not listed as an impurity by the manufacturer, a minute quantity of Na in the target would still be detected because of extremely high SIMS sensitivity for Na. No nitrogen ions were observed in the p-SIMS spectrum and this is attributed to the high ionization potential of nitrogen as well as to the work function.

The intensity of B^+, B_2^+, $(^{11}B+^{10}B)^+$, and BN^+ are plotted as a function of ion energy in Fig. 4. The abscissa is in cps per mA beam current. The isotopic intensities have been combined in this figure to provide total intensities of ions of boron atoms and molecules. Boron atoms can be seen at energies as low as 100 eV but molecules and $(^{10}B+^{11}B)^+$ clusters can be detected starting at 400 eV and BN^+ clusters can be detected starting at 700 eV. The spectral intensities of all positive species increased rapidly from low energy up to 1 keV. Beyond 1 keV, intensities remained essentially constant or increased very slightly. From this figure, it is obvious that B^+ emissions contribute mostly to the total positive secondary ion yield.
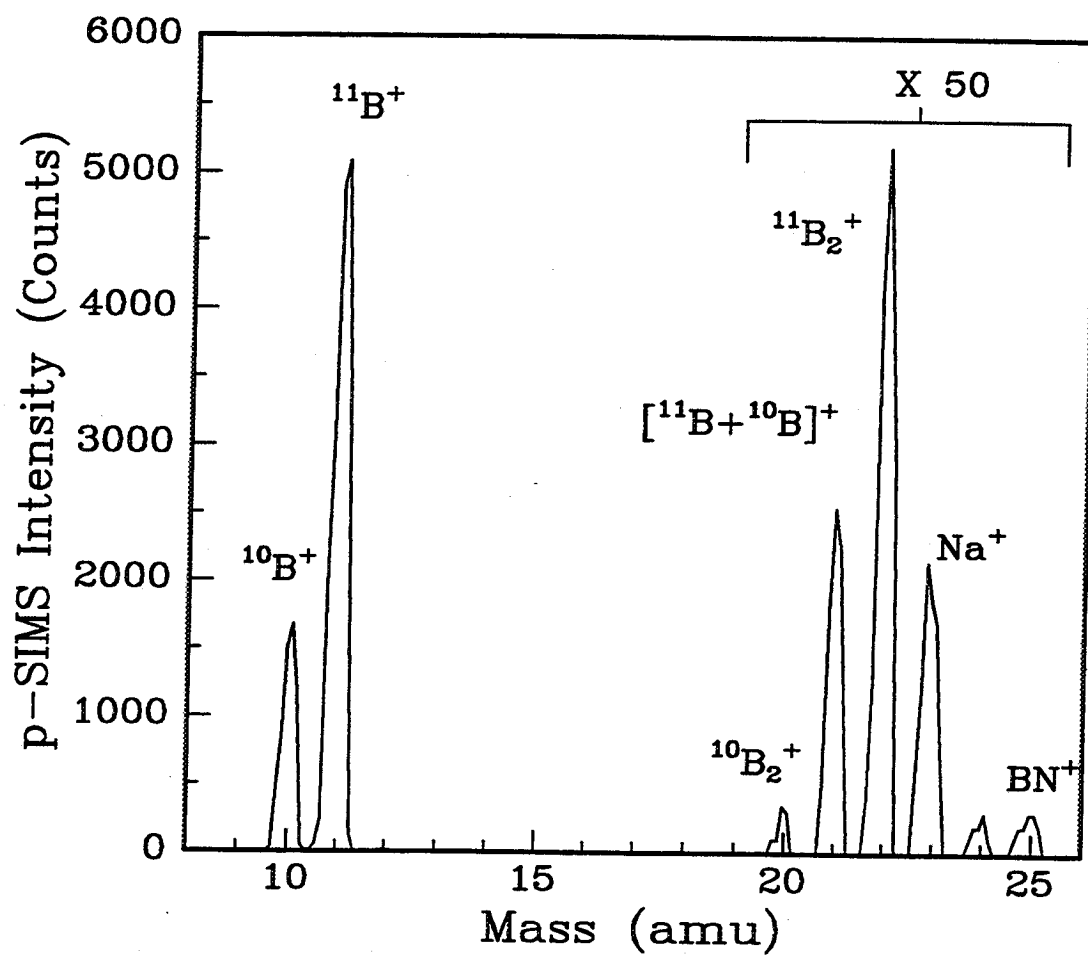
Fig. 3.   Positive SIMS spectrum of boron nitride bombarded by 2 keV xenon ions
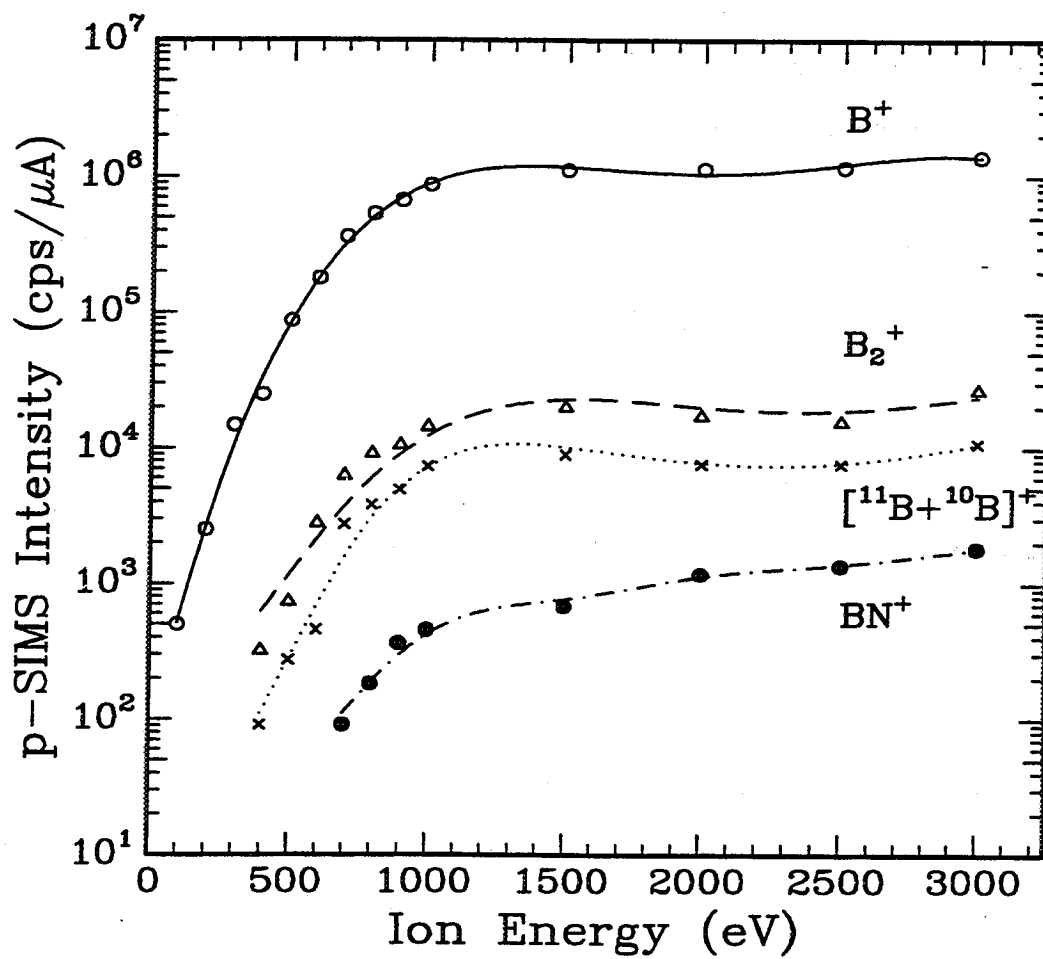
Fig. 4.   Positive SIMS intensities of B^+, B_2^+, $(^{11}B+^{10}B)^+$, and BN^+ as a function of incident ion energy

4.2.2. Negative SIMS spectra

The negative SIMS (n-SIMS) spectrum of boron nitride under 2 keV xenon ion bombardment is shown in Fig. 5. The n-SIMS spectrum exhibits secondary ions of atoms (B^-), molecules (B_2^-) and clusters (BN^-). It also reveals the presence of oxygen at the target surface. The source of F^- signal is attributed to the presence of a minute quantity of F in the target since F, like Na, also has a very high SIMS sensitivity. The BN^- and B^- signals dominate the negative secondary ion spectrum. The two isotopes of boron can also be identified in these two signals. The absence of N^- in the n-SIMS spectrum is expected since elements with zero electron affinity cannot produce negative secondary ions. This also explains the anomalously high B^- yield since an electropositive species such as B does not form negative ions so readily.

Intensities of BN^-, B^- and B_2^- are plotted in Fig. 6 as a function of ion energy. The isotopic intensities have been combined to provide total intensities of boron and boron nitride. BN^- and B^- signals could not be detected below 400 eV whereas B_2^- signal could be detected starting at 600 eV only. In contrast to p-SIMS intensity-energy curves, n-SIMS intensity-energy curves do not exhibit a pronounced knee.

4.2.3. Secondary neutral spectra

The intensity of signals from the secondary neutrals was considerably lower than that from the secondary ions. In general, SNMS signals are less intense than SIMS signals because the SNMS mode of operation suffers from poor ionization efficiencies [37]. Moreover, it is quite likely that a bias voltage was unintentionally created between the target and the analyzer in our experiments via the charge compensation scheme. In the SNMS mode, background signals from carbon and nitrogen caused interference at mass numbers 12 and 14 amu. Background spectra were collected before each SNMS run and were subtracted from SNMS spectra. Background
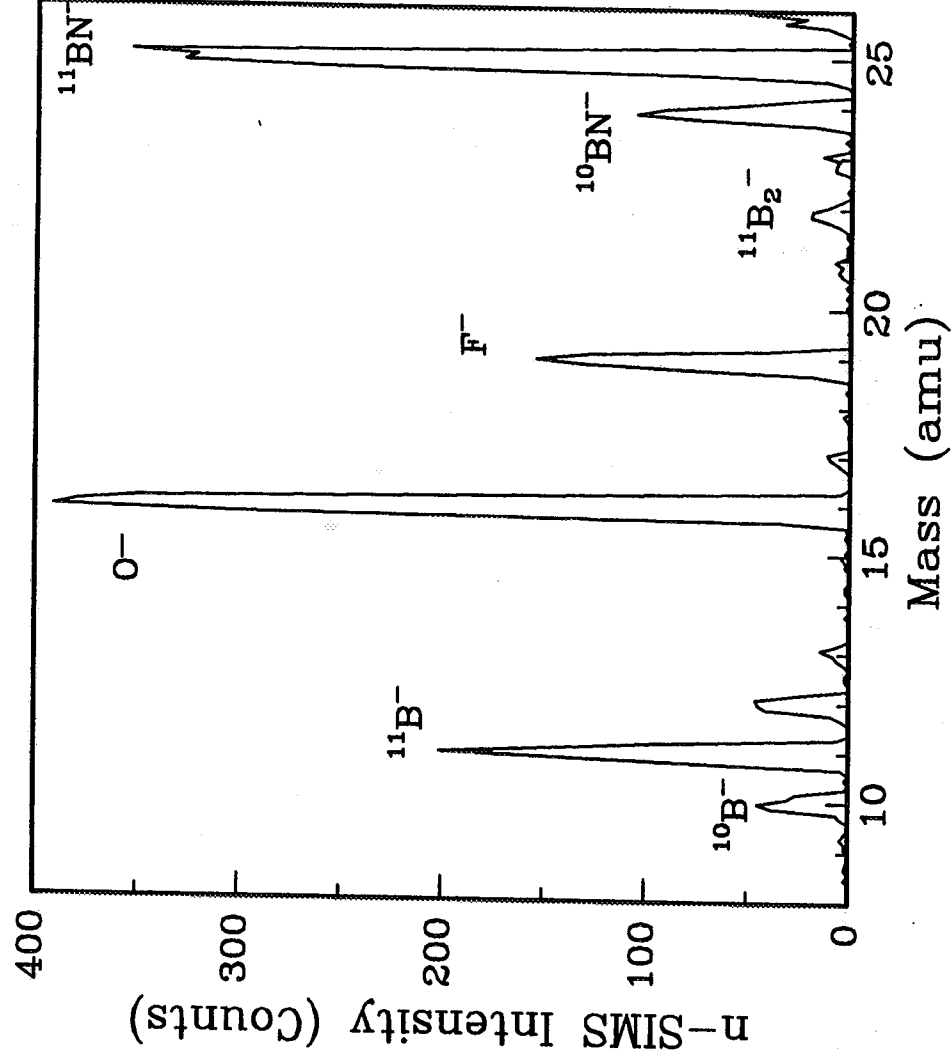
22

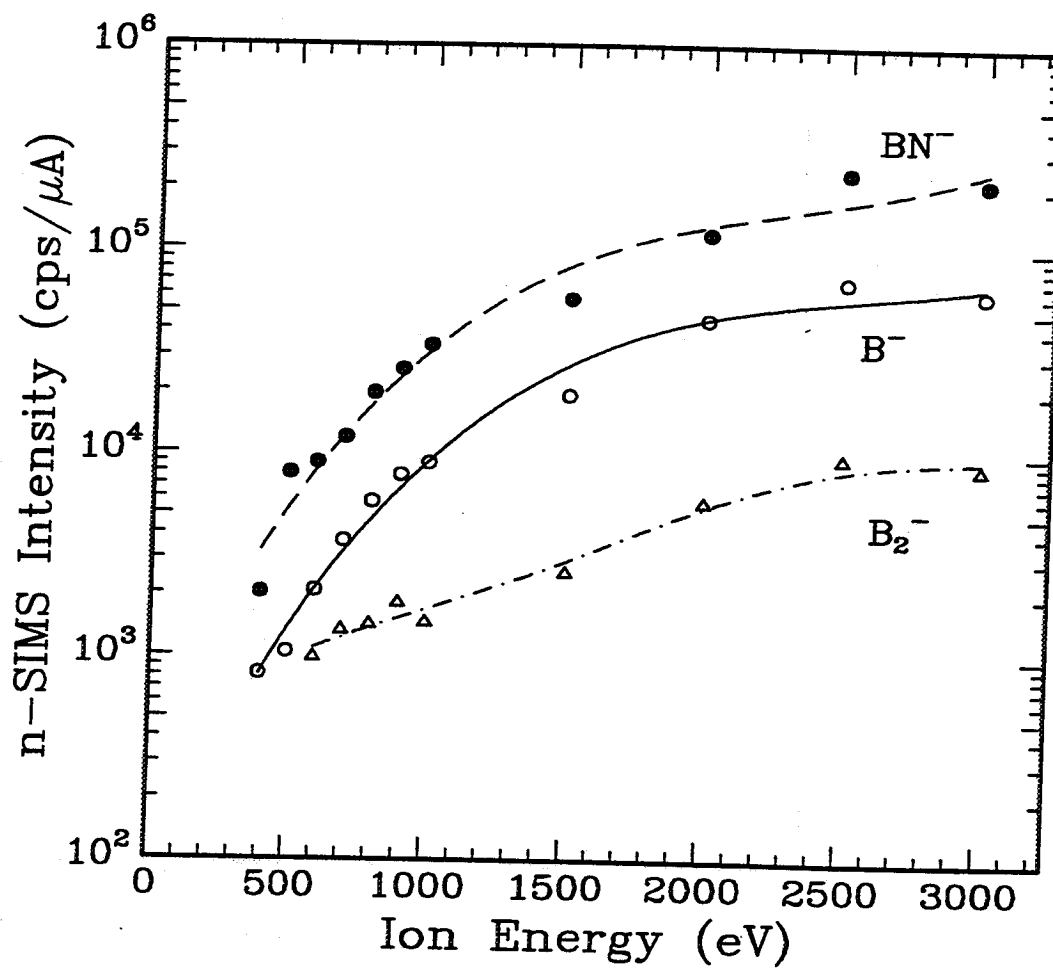Fig. 5. Negative SIMS spectrum of boron nitride bombarded by 2 keV xenon ions

23

Fig. 6.   Negative SIMS intensities of BN⁻, B⁻, and B₂⁻ as a function of incident ion energy

subtracted SNMS spectra taken at 400 eV, 1 keV and 2 keV are presented in Fig. 7. Peaks in SNMS spectra are wider because data were acquired at low mass resolutions to obtain high signal intensities. SNMS spectra also reveal the boron isotopes and ^{14}N. The peak at mass number 12 amu could be due to the presence of carbon at the target surface or from the ^{11}BH cluster.

Spectral intensities (cps/mA) of B and N are shown in Fig. 8 as a function of ion energy. The isotopic intensities have been combined to provide total intensities of boron atoms. Both intensity-energy curves of B and N follow the same pattern. The minimum ion energy which produces a measurable nitrogen yield is 400 eV, whereas boron signals can be observed at 300 eV. The nitrogen signal intensities were particularly low. They show a lot of scatter in the 600 eV to 1 keV energy region, presumably due to statistical effects of subtracting background spectra.

SNMS signal intensities of B and N do not reflect the 1:1 composition of the target. Even in the case of sputtering at the stoichiometric composition rate, SNMS signal intensities of the constituents will generally not reflect the composition of the compound. This is due to the variation in the fraction of the flux of sputtered particles accepted by the spectrometer aperture, the efficiency of neutral-to-ion conversion in the ionizer, and the transmission of ions in the mass spectrometer [38,39]. The relative intensity of signals from boron and nitrogen atoms as a function of ion energy is shown in Fig. 9. It tends to decrease slowly with energy from around 3.6 at 400 eV to 2.0 at 3 keV. Because of the significant higher ionization potential of nitrogen compared to that of boron (14.53 eV for nitrogen versus 8.30 eV for boron), a relatively low detection sensitivity for N is obtained.

The knees appear in intensity-energy curves of both B and N at around 1 keV ion energy. The same characteristic was observed in the p-SIMS intensity-energy curves. However, in the
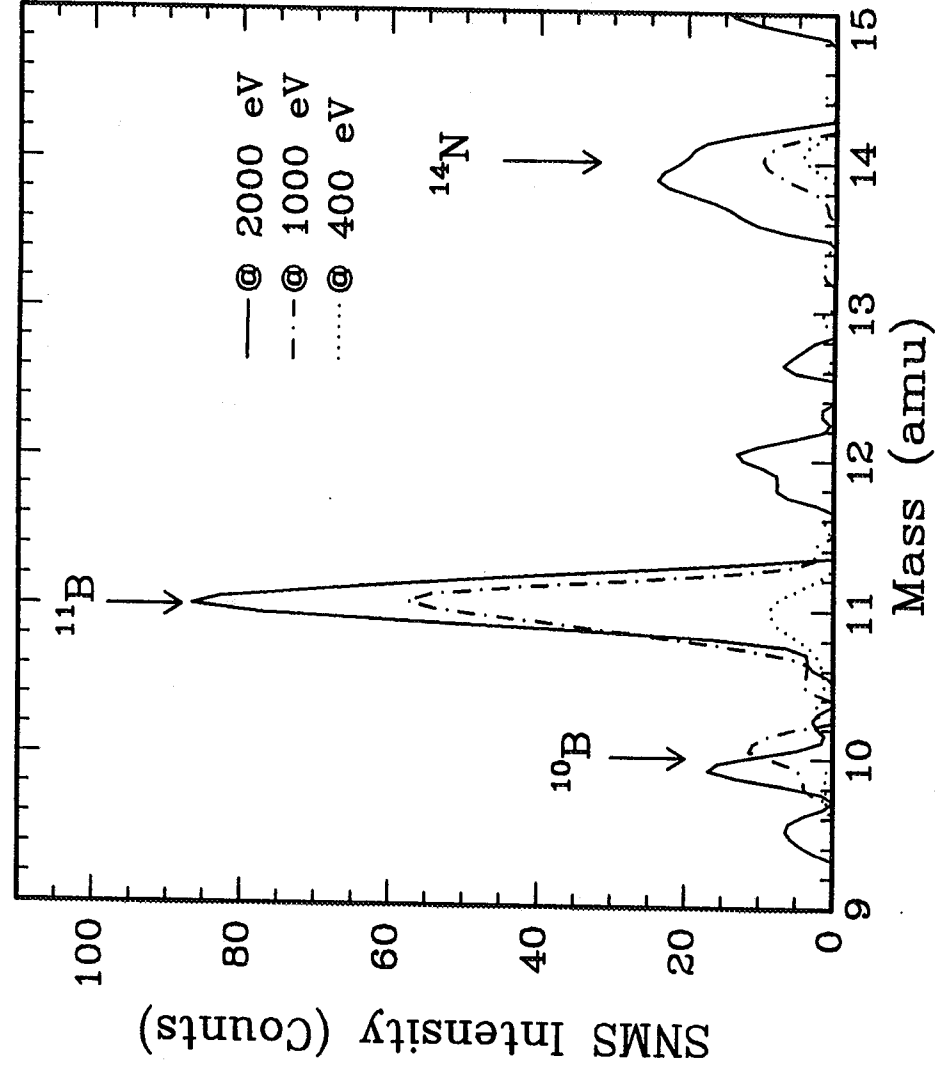
25

Fig. 7. SNMS spectrum of boron nitride bombarded by xenon ions at three different energies
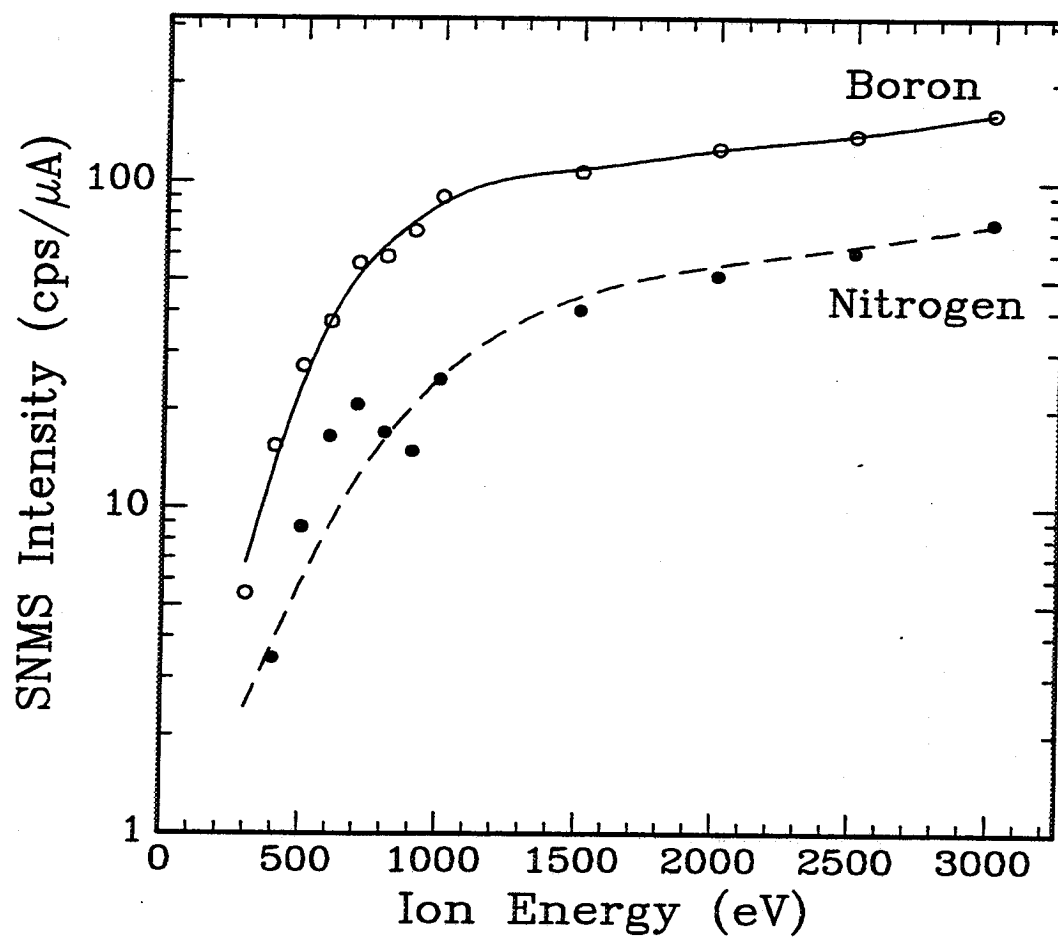
26

Fig. 8.   SNMS intensities of boron and nitrogen atoms as a function of ion energy
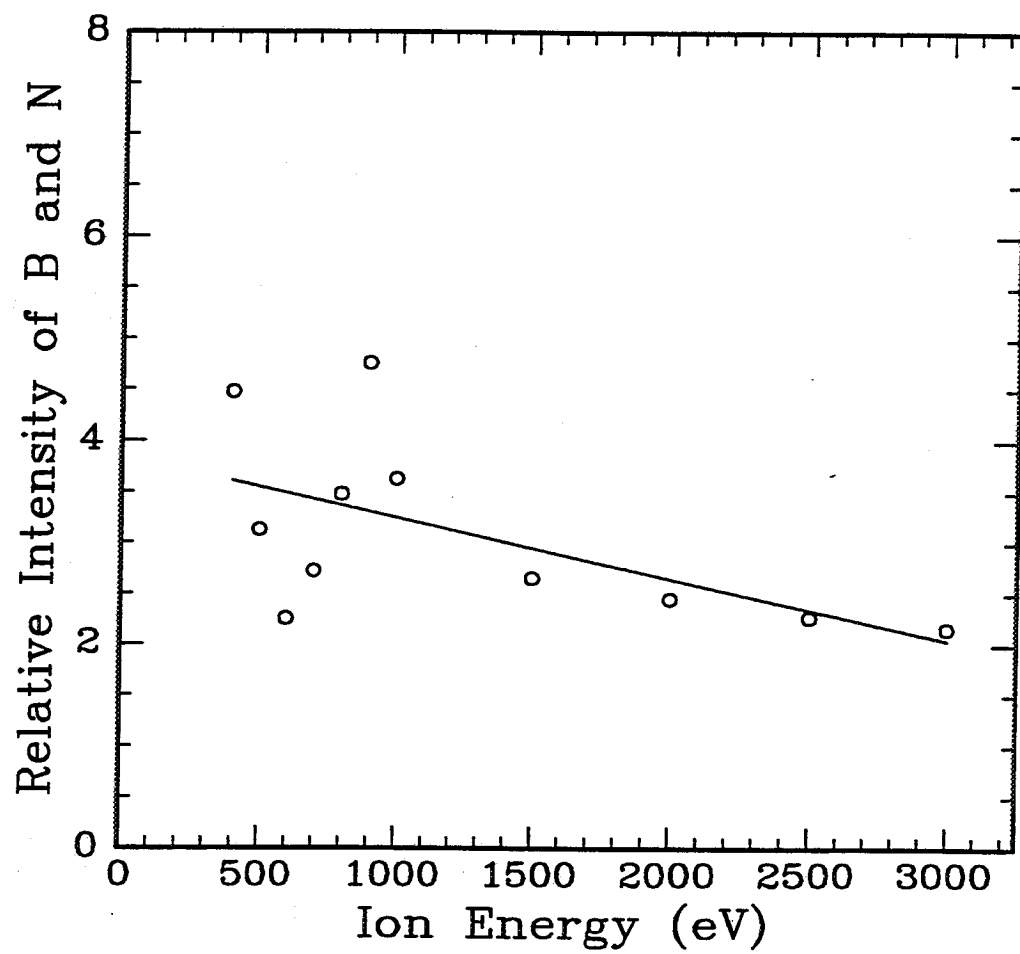
Fig. 9. Relative intensity of boron and nitrogen atoms measured by SNMS versus ion energy

sputtering of medium and heavy elements by ions of argon and xenon, the knees usually appear between 100 to 300 eV [40]. The reason for this difference is attributed to the considerably lower reduced ion energy of the Xe-B pair due to their large mass difference. The sputtering yield depends to a large extent on the reduced nuclear stopping cross section which is a function of the reduced ion energy, ε. It is given by [41]

$$\varepsilon = \frac{0.03255}{Z_1 Z_2 (Z_1^{2/3} + Z_1^{2/3})^{1/2}} \frac{M_2}{(M_1 + M_2)} E \qquad (1)$$

where E is the incident ion energy, Z_1 and M_1 represent the atomic number and mass number of the incident ion, and Z_2 and M_2 represent the atomic number and mass number of the target atom. For two different ion-target combinations such as Xe-B and Xe-Mo, nearly same values of reduced ion energies are obtained at an incident ion energy of 1 keV for the Xe-B pair and 300 eV for the Xe-Mo pair.

4.2.4. Comparison of SNMS and p-SIMS intensity-energy curves of boron

The variation of boron signal intensities measured in SNMS and p-SIMS m odes with ion energy is shown in Fig. 10. The two curves were normalized at 3 keV to allow us to compare their shapes. In the high energy region (800 eV to 3 keV), the two curves agree reasonably well. Below 800 eV, the p-SIMS intensity drops off at a much faster rate than the SNMS intensity.

4.3   Conclusions

SIMS and SNMS were used to investigate the sputtering of boron nitride bombarded by xenon ions with energies ranging from 100 eV to 3 keV. The two boron isotopes, $^{10}B^+$ and $^{11}B^+$,
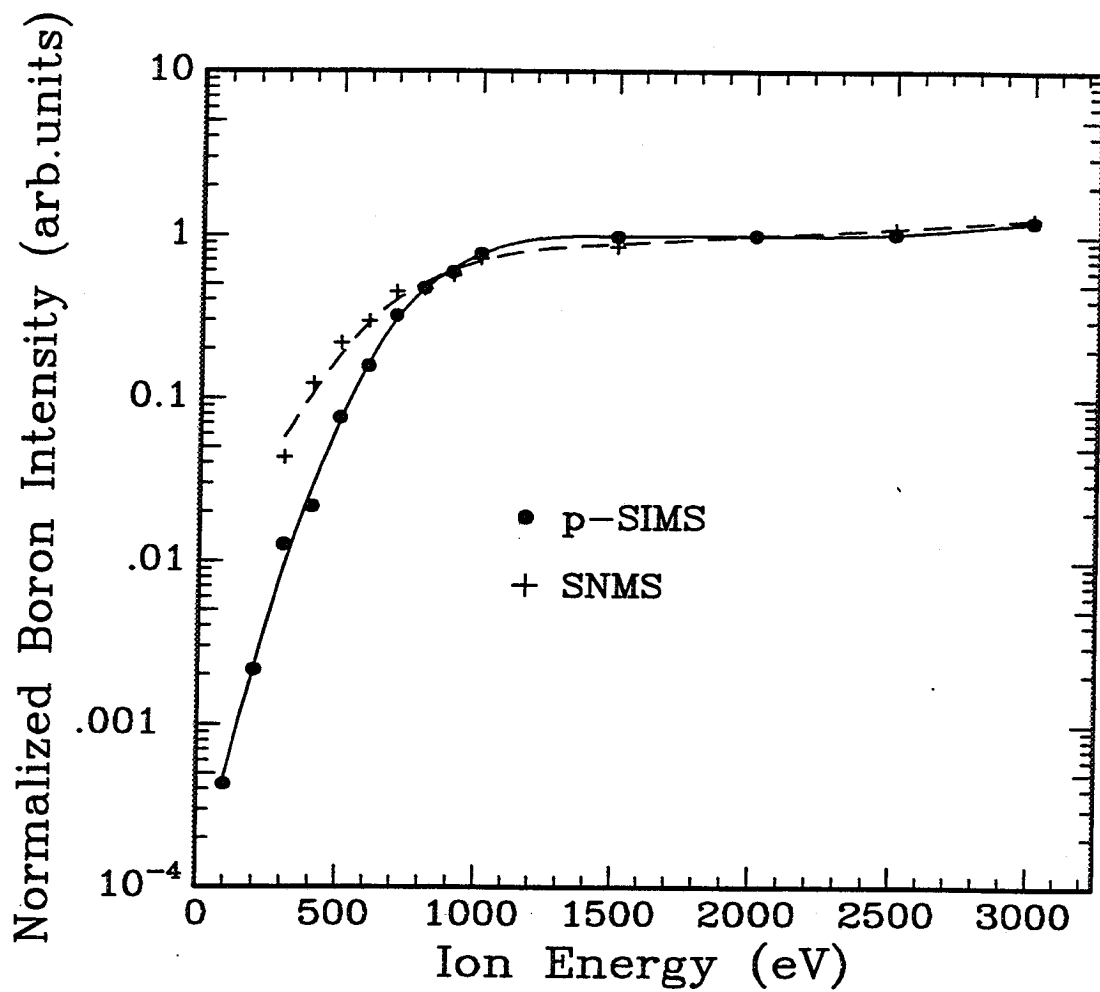
Fig. 10.   Comparison of boron intensities measured in SNMS and p-SIMS modes

dominated the p-SIMS spectra. $^{10}B_2^+$, $^{11}B_2^+$, $(^{10}B+^{11}B)^+$ and BN^+ were also observed in the p-SIMS spectra but in much smaller quantities. $^{10}BN^-$, $^{11}BN^-$, $^{10}B^-$ and $^{11}B^-$ were the major species which were ejected as negative ions from boron nitride. Among the sputtered neutrals, the two isotopes of boron were dominant. Nitrogen could be seen only in the SNMS mode. The shapes of the intensity versus ion energy curves of the sputtered particles were observed to be similar. The knees in p-SIMS and SNMS intensity-energy curves appear at around 1 keV which is significantly higher than 100 to 300 eV energy range at which knees appear in the sputtering of medium and heavy elements by ions of argon and xenon. This difference in the position of the sputter yield knee between boron nitride and heavier targets is due to the reduced ion energy differences.

5. PREFERENTIAL EMISSION OF HEAVY ISOTOPES IN THE SPUTTERING OF BORON NITRIDE

5.1 Introduction

When a multicomponent target is bombarded by energetic particles, a nonstoichiometric composition of sputtered particles is observed due to different sputtering rates of the various constituents of the target. This effect is known as preferential sputtering. Among the sputtered particles are atoms, molecules, and positive and negative ions which are ejected from the surface in ground and various excited states. An understanding of preferential sputtering is relevant to such diverse fields as geo-cosmology, thin film deposition, and secondary ion mass spectrometry. A systematic study of preferential sputtering will also provide further insight into the physics of the sputtering process itself.

A number of fundamental experimental investigations on preferential sputtering from a variety of targets have been made [42-54]. In most of these studies, the targets were bombarded with high energy (> 2 keV) ions, usually at one or two fixed ion energies [42,45-53]. Low energy incident ions have been used in a few studies. Two of these experiments used Hg^+ at 100 eV [43] and 60 to 300 eV [44] using a plasma discharge. In another experiment, 40 to 400 eV Ar^+ beams were used [54]. A variety of other incident ions have been used in studies on preferential sputtering. For example, He^+ [45], N^+ and N_2^+ [46], O^- [47,49], O_2^+ [48], Ne^+ [50], Ar^+ [42,50-53], and Xe^+ [53], have been used as incident ions. The isotope ratios have been measured using a variety of techniques. In some of these studies, the sputtered material was deposited on collector plates and subsequently analyzed [42-44,46,53]. In one case, the target surface was analyzed for changes in isotopic composition after the completion of sputtering [45].

The isotope ratios of secondary ions have also been measured directly by using secondary ion mass spectrometry [47,48-50]. More recently, isotopic composition of sputtered neutrals were measured by secondary neutral mass spectrometry where the sputtered neutral atoms were postionized by electrons in a plasma [51,52,54]. The earlier measurements were generally performed at high ion beam fluence levels while some of the later investigations [49-54] have been conducted using low ion beam fluences ($\approx 1 \times 10^{15}$ ions/cm^2).

In all studies, an enrichment of the lighter isotope in the sputtered flux was observed at small emission angles. As the bombardment is continued, the surface becomes rich in heavy isotopes. Hence, the isotopic composition of the sputtered particles is expected to change with the beam fluence with the enrichment of light isotopes being reduced over time. After prolonged bombardment, usually less than 30 min at keV incident ion energies, one expects some sort of equilibrium to be reached with the composition of the emitted flux remaining unchanged with time. This is referred to as a steady state in the sputtering process.

Several experiments performed at low ion fluences have demonstrated that a steady state is reached in the sputtering process [49,52,53]. In these experiments, the sputtered flux was found to be nearly identical in composition to that of the natural abundance of the bulk target after ion bombardment at keV energies. One study found that a steady state is reached in the sputtered flux of copper after 30 min of sputtering, but the flux remained significantly enriched in light isotopes with respect to the bulk sample composition [47]. The studies performed at higher ion beam fluences have found the sputtered flux to remain enriched in light isotopes. Only one study observed light isotope enrichment in the sputtered flux increasing with time and ultimately reaching an equilibrium [48]. The authors have attributed this to preferential recoil implantation of light isotopes by primary ions.

At larger emission angles, one usually observes preferential emission of heavy isotopes. In one study, isotopic enrichments were measured on Cu, Mo, W and U with Hg^+ ions at energies ranging from 60 to 300 eV [44]. In all cases, except U, it was observed that the sputtered flux was enriched in the light isotopes in the normal direction and in the heavy isotopes in the oblique direction. Preferential emission of heavy isotopes at large angles of emission were also seen in the bombardment of Mo and Ge with 5 keV Ar^+ [51,52] and 5 and 10 keV Ar^+ and Xe^+ [53]. When sputtering of isotopic targets was simulated using a multiple interaction, molecular dynamics model, the variation of isotopic enrichment with the emission angle was demonstrated [55].

When elements were sputtered at low incident ion energies, the isotopic enrichment was found to vary with the primary ion energy. The early study by Olson et al., indicated that in the low energy Hg^+ bombardment of Cu between 60 and 300 eV and of Mo between 100 and 200 eV, the amount of enrichment of light isotopes decreased quite rapidly with increasing energy [44]. In a more recent experiment, isotopic enrichment of the sputtered flux was investigated in the sputtering of Cu and Mo with Ar^+ in the energy range 40 to 440 eV at high fluences [54]. The enrichment was found to vary with incident ion energies with the enrichment decreasing rapidly as the primary ion energy was increased. Similar results have been observed in another study, where Ni and Cu were sputtered by Ar^+ ions at energies ranging from 100 to 500 eV at a moderate fluence level [56].

The analytical treatment developed by Sigmund and co-workers is generally used in analyzing isotopic sputtering [57,58]. It is based on the concept of a linear collision cascade induced by the incident ion [59]. This theory predicts, in the limit of low fluence, an initial enrichment of light isotopes in the sputtered flux. At high primary ion energies, measured enrichments of light isotopes generally agree with those predicted from this theory. Since,

energy and momentum are randomized in a collision cascade, no dependence of isotopic enrichment on the mass and energy of the primary ions, emission angle, and energy of the sputtered particles are obtained from this analytical treatment.

We have observed preferential emission of heavy isotopes at small emission angles when copper was bombarded with xenon ions at energies below 700 eV at moderate fluence level [60]. Moreover, the heavy isotope enrichment was observed to decrease with increasing primary ion energy. Beyond 700 eV, light isotopes were sputtered preferentially with the enrichment remaining nearly constant. This type of behavior was predicted from computer simulations with the TRIM computer code using a Monte Carlo method. This simulation indicated that an enrichment of heavy isotopes is possible at low incident ion energies when the mass of the incident ion is significantly higher than the mass of the target atom [61].

To further explore the preferential sputtering of heavy isotopes by Xe^+ at low primary energies, we have sputtered boron (from a boron nitride target). Boron was chosen because it has two isotopes (masses 10 and 11 u) in the low mass range. In our experiment, we have used xenon ions to bombard a polycrystalline boron nitride target with energies between 100 eV to 1.5 keV. The isotopic enrichment of secondary ions was measured by a quadrupole mass spectrometer. The results of this study are reported here and compared with the results obtained earlier with copper.

5.2   Experimental procedure

The target was first sputter cleaned for 30 minutes using a 2.5 keV rastered ion beam to remove surface impurities. The rastered area was approximately 4 mm x 4 mm in size. The material removed from the target surface during this process is estimated to be 4 nm using a beam fluence of 1.8×10^{16} ions/cm^2. The sputter cleaning process leaves the target surface slightly mass-altered, but this should not have a significant effect on the isotopic enrichment at

low incident ion energies [47,54]. Secondary ions were collected immediately after the sputter cleaning process with the ion beam focused at the center of the cleaned area. Data at each energy were collected over a period of 60 s. The beam fluence was 8.9×10^{15} ions/cm^2 at 100 eV and 1×10^{16} ions/cm^2 at other energies. Since the secondary ion intensities were significantly reduced at lower primary ion energies, the ion optics parameters of the spectrometer were optimized to obtain maximum signal intensities. The width of boron peaks were 0.4 u at FWHM.

5.3   Results and discussion

The $^{10}B^+/^{11}B^+$ isotope ratio, normalized to the natural abundance ratio of these two isotopes, is shown in Fig. 11 as a function of xenon ion energy from 100 eV to 1.5 keV. For comparison, the $^{63}Cu^+/^{65}Cu^+$ isotope ratio obtained earlier is presented in the same figure [60]. The normalized isotope ratios are known as the enrichment factor. The figure shows that the secondary ions of boron are enriched in heavy isotopes at lower primary ion energies. The maximum enrichment factor of heavy isotopes is observed to be 0.901 below 200 eV. The enrichment of heavy isotopes is gradually reduced with increasing primary ion energy. Beyond 350 eV, the secondary ions are observed to be enriched in light isotopes. The enrichment of light isotopes is observed to increase rapidly with primary ion energy in the initial stages until it reaches an asymptotic value of 1.27 at 1.5 keV. A similar trend can be observed in the enrichment factor of the copper isotopes. However, in case of copper, the crossover point from heavy to light isotope enrichment was at 700 eV and the asymptotic light isotope enrichment factor was 1.009.

It should be noted that the secondary ion intensities were low and the measured isotope ratios were normalized to the natural abundance ratios. The large error bars in the data set at lower ion energies are due to these two effects.

The data presented in Fig. 11 can be qualitatively explained by considering the energy transfer between two atoms in a binary collision. In the collision of an ion of mass M_1,
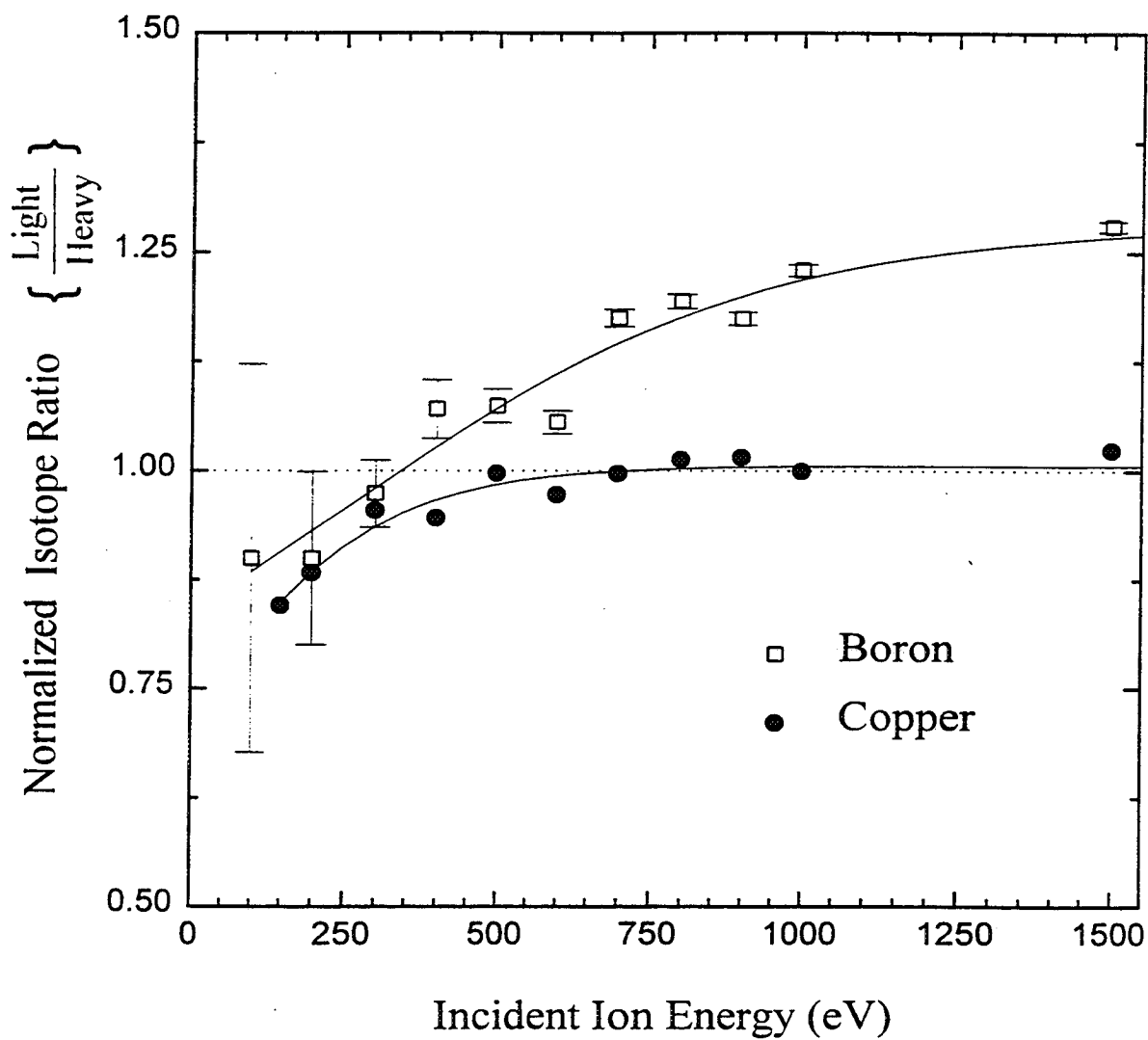
Fig. 11.   Change of $^{10}B^+/^{11}B^+$ and $^{63}Cu^+/^{65}Cu^+$ isotope ratios as a function of xenon ion energy. Data are normalized to the natural abundance ratio of each isotope pair.

possessing kinetic energy E_1, with the target atom of mass M_2, the energy transferred to the target atom T, is given by

$$T = \frac{4 M_1 M_2}{(M_1 + M_2)^2} E_1 \sin^2 \theta / 2$$

$$= \gamma(M_1, M_2) E_1 \sin^2 \theta / 2 \qquad (2)$$

where γ (M_1,M_2) is the energy transfer factor, and θ is the scattering angle of the ion in the center of mass system. The values of γ for the boron and copper isotopes sputtered with xenon ions are listed in Table 1. This table also provides the values of isotopic mass differences $(m_H - m_L)/m_L$ of the isotopic pairs where m_H and m_L are the masses of heavy and light isotope respectively.

Table 1.   Energy transfer factors and isotopic mass differences for xenon ions with boron and copper

Ion-target combination	γ	$(m_H - m_L)/m_L$
Xe - ^{10}B	0.2653	8 %
Xe - ^{11}B	0.2877	8 %
Xe - ^{63}Cu	0.8794	1 %
Xe - ^{65}Cu	0.8880	1 %

At lower incident ion energies, the collision kinematics of a single collision or first few collisions near the surface will likely dominate the emission process. The single-collision or few-collisions occurring are generally not sufficient to produce energy randomization as in the

linear cascade regime. Hence, in the low-energy regime, the energy transferred in binary collisions play a larger role in the particle emission process. Since $\gamma\,(^{11}B) > \gamma\,(^{10}B)$, ^{11}B atoms have higher than average probability to receive more energy than ^{10}B atoms when xenon ions have collisions with boron atoms near the surface and hence, more $^{11}B^{+}$ are expected in the secondary ion flux at lower incident ion energies. The same argument holds true for the composition of the sputtered flux when copper is bombarded by xenon ions at lower energies.

With higher incident ion energies, the bombarding ion penetration into the target is deeper and collision cascades are expected to be more fully developed. The cross section for energy transfer in elastic scattering increases with decreasing mass of the struck particle. Therefore, light isotopes have higher than average probability of being hit, and lower than average probability of loosing energy after being set in motion [58]. So the sputtering yields of $^{10}B^{+}$ and $^{63}Cu^{+}$ are expected to be higher than those of $^{11}B^{+}$ and $^{65}Cu^{+}$ at higher primary ion energies. Moreover, since isotopic mass differences for boron is much higher than that of copper, the proportion of light isotope in the sputtered flux of boron is expected to be much higher than the proportion of light isotopes in the sputtered flux of copper. The higher values of the light isotope enrichment factors observed for boron compared to copper support this argument.

From the argument presented in the previous paragraphs, the enrichment of heavy isotopes is expected to be higher at lower ion energies when the mass of the incident ion is significantly higher than the mass of the target atom. With increasing primary ion energy, an increasing amount of the light isotope is likely to be sputtered until at some point, the sputtered flux is enriched in light isotopes.

At a given primary ion energy, xenon is expected to penetrate deeper into boron nitride than copper because of the lighter masses of the constituents of boron nitride. For example, a TRIM calculation showed that the range of 200-eV xenon ions is 1.6 nm in boron and 0.7 nm in copper. Since at a given energy, the xenon ions have a higher probability to penetrate deeper into boron nitride, the collision cascades are expected to form at a lower ion energy in boron

nitride. Hence, the crossover point from heavy to light isotope enrichment is expected at lower primary ion energy in boron nitride compared to copper as was observed in our experiments.

When a target containing isotopes having adjacent masses (such as boron) is sputtered, one needs to be careful about the interference due to the formation of hydrides. Shimizu and Hart examined the hydride interference problem for several elements, including boron [47]. They found the metal to metal hydride ratio higher than 100 in all cases. In our system also, the hydride interference was estimated to be less than 1%. The masses of copper isotopes are separated by two units and hence, interference from the formation of hydrides of copper was not a major problem.

Isotopic enrichments from elemental boron targets have been measured with 100 keV Ar^+ and Ne^+ ions [50] as well as 13.2 keV O^- ions [47]. In the first study, a light isotope secondary ion enhancement in the sputtered flux was observed at low beam fluences. With continued sputtering, its value decreased to reflect the bulk composition of the target when the steady state was reached. In the second study, the researchers analyzed the energy of the secondary ions and found a significant dependence of isotopic ratio on the energy of the analyzed ion.

When elements containing isotopes are sputtered, kinematics effects due to isotopic mass differences play a significant role in the preferential emission of one isotope over the other. The study of preferential sputtering in compounds can be complicated by the existence of chemical forces between components of the target materials. It is difficult to estimate the relative importance of collisional and chemical effects when a compound is sputtered. There is some evidence though that in sputtering at low energies collisional effects tend to dominate over chemical ones. Larger preferential sputtering was observed when compounds such as TaC, Ta_2O_5, and TiN were sputtered at low ion energies (< 2keV) [62,63].

The arguments presented earlier are supported by two experiments where low-energy argon ions have been used to sputter copper, molybdenum and nickel [54,56]. The values of γ for the isotopes of these elements sputtered with argon ions are listed in Table 2. In all cases,

γ (light isotope) is grater than γ (heavy isotope). Hence, in the sputtering of copper, molybdenum and nickel by low-energy argon ions, the sputtered particle flux is always expected to be enriched in light isotopes which was observed experimentally. The different behavior of the enrichment factor in sputtering with argon and xenon ions is clearly seen in Fig. 12 where normalized isotope ratios in Ar^+-Cu and Xe^+-Cu sputtering are presented for primary ion energies below 500 eV.

Table 2. Energy transfer factor for argon ions with nickel, copper and molybdenum

Ion-target combination	γ
Ar - ^{58}Ni	0.966
Ar - ^{60}Ni	0.960
Ar - ^{63}Cu	0.950
Ar - ^{65}Cu	0.943
Ar - ^{92}Mo	0.844
Ar - ^{100}Mo	0.816

5.4   Conclusions

An experimental investigation in isotopic enrichment of secondary ions of boron at low incident ion energies and moderate fluence levels has been conducted. Boron nitride was sputtered with xenon ions at energies ranging from 100 eV to 1.5 keV. The secondary ions of boron were measured by a quadrupole mass spectrometer. The secondary ions were observed to be enriched in the heavy isotope at lower ion energies. The proportion of heavy isotopes in the sputtered secondary ion flux was found to decrease with increasing primary ion energy from 100 to 350 eV. Beyond 350 eV, light isotopes were sputtered preferentially. The light isotope
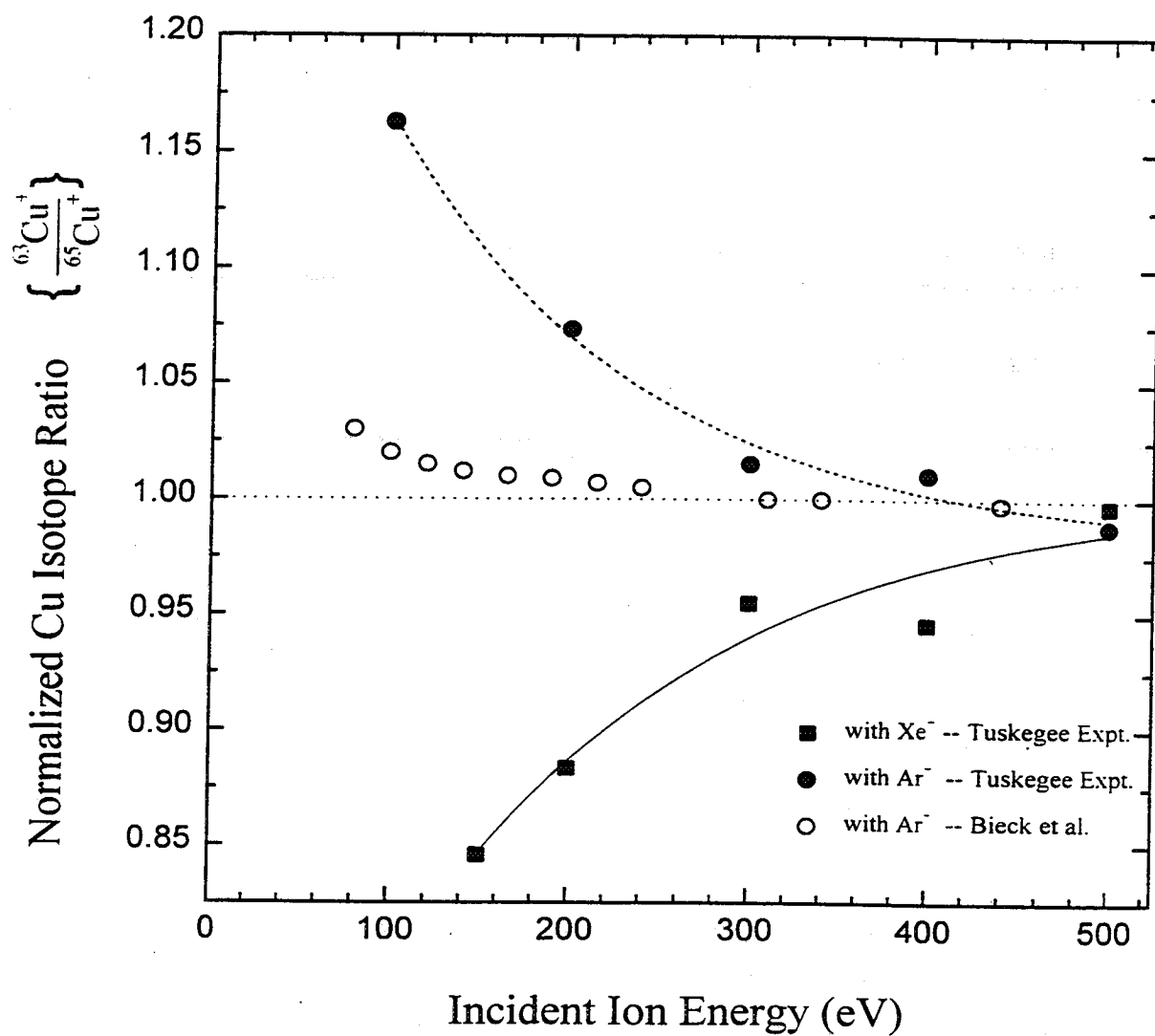
Fig. 12.   Normalized isotope ratio of copper as a function of argon and xenon ion energy.

enrichment factor was observed to increase with increasing energy and reach an asymptotic value of 1.27 at 1.5 keV.

6. REFERENCES

1.   Buarova, A. I., Kim, V., Maslenikov, N. A. and Morozov, A. I., "Physical Process and Characteristics of Stationary Plasma Thrusters with Closed Electron Drift", IEPC-91 -079, (1991).

2.   Brophy, J. R., Barnett, J. W., Sankovic, J. M. and Barnhart, D. A., "Performance of the Stationary Plasma Thruster: SPT-100", AIAA-92-3155, (1992).

3.   Sankovic, J. M., Hamley, J. A. and Haag, T. W., "Performance Evaluation of the Russian SPT-100 Thruster at NASA LeRC", NASA Technical Memorandum 106401, (1993).

4.   Sankovic, J. M., Haag, T. W. and Manzella, D. H., "Performance Evaluation of a 4.5 kW SPT Thruster", IEPC-95-30, (1995).

5.   Garner, C. E., Brophy, J., Polk, J. and Pless, L., "Cyclic Performance and Wear Test of the SPT-100", AIAA-95-2667, (1995).

6.   Myers, R. M. and Manzella, D. A., "Stationary Plasma Thruster Plume Characteristics", IEPC-93-096, (1993).

7.   Manzella, D. A., "Stationary Plasma Thruster Plume Emissions", IEPC-93-097, (1993).

8.   Absalamov, S. K. et al., "Measurement of Plasma Parameters in the Stationary Plasma Thrusters (SPT-100) Plume and Its Effect on the Spacecraft Components", AIAA-92-3156, (1992).

9.   Pencil, E. J., " Preliminary Far-Field Plume Sputtering Characterization of the Stationary Plasma Thruster (SPT-100)", IEPC-93-098, (1993).

10. Randolph, T., Pencil, E. and Manzella, D. H., "Far- Field Plume Contamination and Sputtering of the Stationary Plasma Thruster", AIAA-94-2855, (1994).

11. Pencil, E. J., Randolph, T. and Manzella, D. H., "End- of- Life Stationary Plasma Thruster Far-Field Plume Characterization", AIAA-96-2709, (1996).

12. Trehan, R., Lifshitz, Y., and Rabalais, J., "Auger and X-ray Electron Spectroscopy Studies of h-BN, c-BN, and N_2^+ Ion Irradiation of Boron and Boron Nitride" J. Vac. Sci.

Technol. **A8**, 4026 (1990).

13. Shimizu, R., "Preferential Sputtering", Nucl. Instr. Meth Phys. Res. **B18**, 486 (1987).

14. Zalm, P. C., "Secondary Ion Mass Spectrometry", Vacuum, **45**, 753 (1994).

15. Oechsner, H., Schoof, H., and Stumpe, E., "Sputtering of Ta_2O_5 by Ar^+ Ions Energies Below 1 keV", Surf. Sci. **76**, 343 (1978).

16. Mamoru, N., Hiroyasu, S., and Takaaki, K., "Low Voltage and High Speed Operating Electrostatic Wafer Chuck Using Sputtered Tantalum Oxide Membrane", J. Vac. Sci. Technol. **A12**, 2834 (1994).

17. Dang, T. A., Meyer, G. and Cuddy, J., " Depth Profiling of Nonconductive Powders Using Low- Pressure Radio- Frequency Plasma", J. Vac. Sci. Technol. **A11**, 2364 (1993).

18. Fichtner, M., Goschmick, J., Schrimd, U. C., Schweiker, J. and Ache, H., "Quantitative Analysis of Ionic Solids by Secondary Neutral Mass Spectrometry", J. Vac. Sci. Technol. **A10**, 362 (1992).

19. Goschmick, J., Schuricht, J., Schweiker, A. and Ache, H., "Sputter Yields and Erosion Rates for Low Energy Ion Bombardment of Multielemental Powders", Nucl. Instr. Meth. Phys. Res. **B83**, 339 (1993).

20. Sroubek, Z. and Oechsner, H., " Study of Ionization Processes in Sputtering of LiF", Surf. Sci. **311**, 263 (1994).

21. Varga, P., Diebold, U. and Watte, D., "Electronic Effects in Low- Energy Ion Sputtering of LiF", Nucl. Instr. Meth. Phys. Res. **B58**, 417 (1991).

22. Priggemeyer, S. and Heiland, W., "Sputtering and Crater Formation in Oxidic Materials due to Ion Induced Sputtering Dependent on Energy", Nucl. Instr. Meth. Phys. Res. **B78**, 198 (1993).

23. Priggemeyer, S., Bomermann, J., Alber, T., Koschmieder, H. and Heiland, W., " Sputtering Effects of Craters ", Nucl. Instr. Meth. Phys. Res. **B88**, 244 (1994).

24. Neidlart, T., Toth, Z., Hochhold, M., Schimd, M. and Varga, P., "Total Sputter

Yield of LiF Induced by Hyperthermal Ions Measured by a Quartz Microbalance", Nucl. Instr. Meth. Phys. Res., **B90**, 496 (1990).

25. Betz, G. and Husinsky, W., "Sputtering of Insulators," Nucl. Instr. Meth. Phys. Res. <u>B32</u>, 331 (1988).

26. Weeiser, M., "Quantitative Investigation of the Removal of Glass Material by Low Energy Ion Beams with the Use of Optical Interferometry", Nucl. Instr. Meth. Phys. Res. **B80/81**, 1174 (1993).

27. Ellegaard, O., Schou, J., Soreensn, H., Pedrys, R. and Warczak, B., "Sputtering of Solid Nitrogen by keV Helium Ions", Nucl. Instr. Meth. Phys. Res. **B78**, 192 (1993).

28. Postawa, Z., Kolodziej, J., Czuba, P., Piakkowski, P., Szymonski, M., Bilanska, E., Camra, J., Ciach, T., Faryna, M. and Rakowska, A., "Secondary Ion Production By Electron and Ion Bombardment of Alkali Halides", Nucl. Instr. Meth. Phys. Res. **B78**, 314 (1993).

29. Szymrislki, M., Poradzisz, A., Czuba, P., Kolodziej J., Frie, J., Tanoric, L. and Tanovic, N., "Electron Stimulated Desorption of Neutral Species From (100) KCl Surfaces", Surf. Sci. **260**, 295 (1992).

30. Hamagaki, M., Kalo, S., Hara, T. and Hayashi, S., " SNMS-SNART: Focusing on Insulator Analysis", Vacuum, **41**, 1730 (1990).

31. Pignolet, A., Roy, R., Doyle, J., and Cuomo, J., "Model of Lead Loss in $Pb(Mg_xNb_{1-x})O_z$ Ion Beam Sputtered Thin Films", J. Vac. Sci. Technol. **A12**, 2840 (1994).

32. Jun. A., Ko, H., Narbutovskih, M., Sheats, J., and Tibbs, K., " Superconducting $Ba_{1-x}K_xBiO_3$ Thin Films and Junctions", J. Appl. Phys., **74**, 4620 (1993).

33. Jongmin, K., Jeffrey, J., Muamer Z., and Douglas, G., "Depth Profiling Analysis of Aluminum Oxidation During Film Deposition in a Conventional High Vacuum System", J. Vac. Sci. Technol. **A12**, 3062, (1994).

34. Wehner, G., "The Aspects of Sputtering in Surface Analysis Methods", in Methods of Surface Analysis, ed. Czanderna, A., Elsevier, New York, (1975), p. 14.

35. Kouvetakis, J., Patel, V., Miller, C., and Beach, D., " Composition and Structure of BN Films Deposited by Chemical Vapor Deposition from Borazine", J. Vac. Sci. Technol. **A8**, 3929 (1990).

36. Lifshitz, Y., Kasi, S., Rabalais, J., and Eckstein, W., "Subplantation Model for Film Growth from Hyperthermal Species", Phys. Rev. **B41**, 10468 (1990).

37. Gnaser, H., Fleischhauer, J. and Hofer, W.O., "Analysis of Solids by Secondary Ion and Sputtered Neutral Mass Spectrometry", Appl. Phys. **A37,** 211 (1985).

38. Oechsner, H., "Recent Applications of Secondary Neutral Mass Spectrometry for Quantitative Analysis of Homogeneous and Structured Samples", Nucl. Instr. Meth. **B33**, 91 (1988).

39. Wucher, A., Novak, F. and Reuter, W., "Relative Elemental Sensitivity Factors in Secondary Neutral Mass Spectrometry", J. Vac. Sci. Technol. **A6**, 2265 (1988).

40. Yamamura, Y. and Tawara, H., "Energy Dependence of Ion-Induced Sputtering Yields from Monatomic Solids at Normal Incidence", At. Data and Nucl. Data Table, **62**, 149 (1996).

41. Matsunami, N., Yamamura, Y., Itakawa, Y., Itoh, N., Kazumata, Y., Miyagawa, S., Morita, K., Shimizu, R. and Tawara, H., "Energy Dependence of Ion-Induced Sputtering Yields of Monatomic Solids" At. Data and Nucl. Data Table, **31**,1 (1984).

42. Fluit, J. M., Friedman, L., Boerboom, A. J. H. and Kistemaker, J., "Isotopic Fractionation of Lithium in Sputtering", J. Chem. Phys. **35**, 1143 (1961).

43. Wehner, G. K., "Isotope Enrichment in Sputter Deposits", Appl. Phys. Lett. **30**, 185 (1977).

44. Olson, R. R., King, H. E. and Wehner, G. K., "Mass Effects on Angular Distribution of Sputtered Atoms", J. Appl. Phys. **50**, 3677 (1979).

45. Arai, O., Tazawa, Y., Shmamura, T. and Kobayasyi, T., "Isotopic Fractionation of

Magnesium Sputtered by 2 keV He$^+$ Ions", Japan. J. Appl. Phys. **18**, 1231 (1979).

46. Russell, W. A., Papanastrassiou, D. A. and Tombrello, T. A., "The Fractionation of Ca Isotopes by Sputtering", Rad. Eff. **50,** 41 (1980).

47. Shimizu, N. and Hart, S. R., "Isotope Fractionation in Secondary Ion Mass Spectrometry", J. Appl. Phys. **52,** 1303 (1982).

48. Okano, J., Ochiai, T. and Nishimura, H., "Ion-Beam Induced Isotope Composition Changes in Metal Surfaces and Recoil Implantation" Appl. Surf. Sci. **22/23,** 72 (1985).

49. Gnaser, H. and Hutcheon, I. D., "Preferential Emission of Lighter Isotopes in the Initial Stage of Sputtering", Surf. Sci. **195,** 499 (1988).

50. Baumel, L. M., Weller, M. R., Weller, R. A. and. Tombrello, T. A., "Isotopic Composition of Boron Secondary Ions as a Function of Ion-Beam Fluence", Nucl. Instr. Meth. Phys. Res. **B34**, 427 (1988).

51. Gnaser, H. and Oechsner, H., "Preferential Sputtering of Isotopes: Fluence and Emission-Angle Dependence", Phys. Rev. Lett. **63,** 2673 (1989).

52. Gnaser, H. and Oechsner, H., "Isotopic Mass Effects in Sputtering: Dependence on Fluence and Emission Angle", Nucl. Instr. Meth. Phys. Res. **B48**, 544 (1990).

53. Weathers, D. L., Spicklemirre, S. J., Tombrello., T. A., Hutcheon, I. D. and Gnaser, H., "Isotopic Fractionation in the Sputtering of ^{92}Mo-^{100}Mo Targets", Nucl. Instr. Meth. Phys. Res. **B73,** 135 (1993).

54. Bieck, W., Gnaser, H. and Oechsner, H., "Isotopic Mass Effects in Low-Energy Sputtering of Copper and Molybdenum", Nucl. Instr. Meth. Phys. Res. **B101,** 33 (1995).

55. Shapiro, M. H., Haff, P. K., Tombrello, T. A. and Harrison, D. E., "Simulation of Isotopic Mass Effects in Sputtering", Nucl. Instr. Meth. Phys. Res. **B12,** 137 (1985).

56. Zhang, J., Shutthanandan, V. and Ray, P. K., "Isotopic Enrichment in Sputtering at Low Incident Energies", in <u>Secondary Ion Mass Spectrometry SIMS XI,</u> ed. G. Gillen et al., John Wiley & Sons, Chichester, (1998). p.75.

57. Sigmund, P., "Preferential Sputtering from Isotopic Mixtures and Alloys of Near-Neighbor Elements", Nucl. Instr. Meth. Phys. Res. **B18,** 375 (1987).

58. Sigmund, P., Oliva. A. and Falcone. F., "Sputtering of Multicomponent Materials: Elements of a Theory", Nucl. Instr. Meth. **194,** 541 (1982).

59. Sigmund, P., "Theory of Sputtering: Sputtering Yield of Amorphous and Polycrystalline Targets", Phys. Rev. **184,** 383 (1969).

60. Shutthanandan, V., Zhang, J. and Ray, P. K., "Preferential Sputtering of Heavy Isotopes at Low Incident Ion Energies", Surf. Sci. **392,** L11 (1997).

61. Eckstein, W. and Biersack, J. P., "Computer Simulation of Two-Component Target Sputtering", Appl. Phys. **A37,** 95 (1985).

62. Taglauer, E. and Heiland, W., "Mass and Energy Dependence of the Equilibrium Surface Composition of Sputtered Tantalum Oxide", Appl. Phys. Lett. **33,** 95 (1978).

63. Taglauer, E., "Surface Modifications due to Preferential Sputtering", Appl. Surf. Sci. **13,** 80 (1982).

REPORT DOCUMENTATION PAGE

1. AGENCY USE ONLY (Leave blank)	2. REPORT DATE	3. REPORT TYPE AND DATES COVERED
	January 1999	Final Contractor Report

4. TITLE AND SUBTITLE

Low–Energy Sputtering Studies of Boron Nitride with Xenon Ions

5. FUNDING NUMBERS

WU–632–1B–1B–00
NAG3–1582

6. AUTHOR(S)

P.K. Ray and V. Shutthanandan

7. PERFORMING ORGANIZATION NAME(S) AND ADDRESS(ES)

Mechanical Engineering Department
Tuskegee University
Tuskegee, Alabama 36088

8. PERFORMING ORGANIZATION REPORT NUMBER

E–11521

9. SPONSORING/MONITORING AGENCY NAME(S) AND ADDRESS(ES)

National Aeronautics and Space Administration
Lewis Research Center
Cleveland, Ohio 44135–3191

10. SPONSORING/MONITORING AGENCY REPORT NUMBER

NASA CR—1999-208873

11. SUPPLEMENTARY NOTES

Project Manager, Eric Pencil, NASA Lewis Research Center, organization code 5430, (216) 977–7463.

12a. DISTRIBUTION/AVAILABILITY STATEMENT

Unclassified - Unlimited
Subject Category: 72   Distribution: Nonstandard

This publication is available from the NASA Center for AeroSpace Information, (301) 621–0390.

12b. DISTRIBUTION CODE

13. ABSTRACT (Maximum 200 words)

Sputtering of boron nitride with xenon ions was investigated using secondary ion (SIMS) and secondary neutral (SNMS) mass spectrometry. The ions generated from the ion gun were incident on the target at an angle of 50° with respect to the surface normal. The energy of ions ranged from 100 eV to 3 keV. A flood electron gun was used to neutralize the positive charge build–up on the target surface. The intensities of sputtered neutral and charged particles, including single atoms, molecules, and clusters, were measured as a function of ion energy. Positive SIMS spectra were dominated by the two boron isotopes whereas BN^- and B^- were the two major constituents of the negative SIMS spectra. Nitrogen could be detected only in the SNMS spectra. The intensity–energy curves of the sputtered particles were similar in shape. The knees in p–SIMS and SNMS intensity–energy curves appear at around 1 keV which is significantly higher that 100 to 200 eV energy range at which knees appear in the sputtering of medium and heavy elements by ions of argon and xenon. This difference in the position of the sputter yield knee between boron nitride and heavier targets is due to the reduced ion energy differences. The isotopic composition of secondary ions of boron were measured by bombarding boron nitride with xenon ions at energies ranging from 100 eV to 1.5 keV using a quadrupole mass spectrometer. An ion gun was used to generate the ion beam. A flood electron gun was used to neutralize the positive charge buildup on the target surface. The secondary ion flux was found to be enriched in heavy isotopes at lower incident ion energies. The heavy isotope enrichment was observed to decrease with increasing primary ion energy. Beyond 350 eV, light isotopes were sputtered preferentially with the enrichment increasing to an asymptotic value of 1.27 at 1.5 keV. The trend is similar to that of the isotopic enrichment observed earlier when copper was sputtered with xenon ions in the same energy range.

14. SUBJECT TERMS

Sputtering; Boron nitride; Secondary ion mass spectrometry; Secondary neutral mass spectrometry

15. NUMBER OF PAGES

55

16. PRICE CODE

A04

17. SECURITY CLASSIFICATION OF REPORT	18. SECURITY CLASSIFICATION OF THIS PAGE	19. SECURITY CLASSIFICATION OF ABSTRACT	20. LIMITATION OF ABSTRACT
Unclassified	Unclassified	Unclassified	